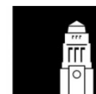

UNIVERSITY OF LEEDS

This is a repository copy of *Quantitative Evaluation of the Carbon Hybridization State by Near Edge X-Ray Absorption Fine Structure Spectroscopy.*.

White Rose Research Online URL for this paper:
http://eprints.whiterose.ac.uk/95811/

Version: Accepted Version

Article:

Mangolini, F, McClimon, JB and Carpick, RW (2016) Quantitative Evaluation of the Carbon Hybridization State by Near Edge X-Ray Absorption Fine Structure Spectroscopy. Analytical Chemistry, 88 (5). pp. 2817-2824. ISSN 0003-2700

https://doi.org/10.1021/acs.analchem.5b04525

Reuse

Unless indicated otherwise, fulltext items are protected by copyright with all rights reserved. The copyright exception in section 29 of the Copyright, Designs and Patents Act 1988 allows the making of a single copy solely for the purpose of non-commercial research or private study within the limits of fair dealing. The publisher or other rights-holder may allow further reproduction and re-use of this version - refer to the White Rose Research Online record for this item. Where records identify the publisher as the copyright holder, users can verify any specific terms of use on the publisher's website.

Takedown

If you consider content in White Rose Research Online to be in breach of UK law, please notify us by emailing eprints@whiterose.ac.uk including the URL of the record and the reason for the withdrawal request.

eprints@whiterose.ac.uk
https://eprints.whiterose.ac.uk/

Quantitative Evaluation of the Carbon Hybridization State by Near Edge X-Ray Absorption Fine Structure Spectroscopy

Filippo Mangolini[1,*], *J. Brandon McClimon*[2], *Robert W. Carpick*[3]

[1] Institute of Functional Surfaces, School of Mechanical Engineering, University of Leeds, Leeds, LS2 9JT, UK

[2] Department of Materials Science and Engineering, University of Pennsylvania, Philadelphia, Pennsylvania 19104, USA

[3] Department of Mechanical Engineering and Applied Mechanics, University of Pennsylvania, Philadelphia, Pennsylvania 19104, USA

* Author to whom correspondence should be addressed. Electronic email: f.mangolini@leeds.ac.uk

ABSTRACT

The characterization of the local bonding configuration of carbon in carbon-based materials is of paramount importance since the properties of such materials strongly depend on the distribution of carbon hybridization states, the local ordering, and the degree of hydrogenation. Carbon 1s near edge X-ray absorption fine structure (NEXAFS) spectroscopy is one of the most powerful techniques for gaining insights into the bonding configuration of near-surface carbon atoms. The common methodology for quantitatively evaluating the carbon hybridization state using C1s NEXAFS measurements, which is based on the analysis of the sample of interest and of a highly ordered pyrolytic graphite (HOPG) reference sample, was reviewed and critically assessed, noting that inconsistencies are found in the literature in applying this method. A theoretical rationale for the specific experimental conditions to be used for the acquisition of HOPG reference spectra is presented together with the potential sources of uncertainty and errors in the correctly computed fraction of sp^2-bonded carbon. This provides a specific method for analyzing the distribution of carbon hybridization state using NEXAFS spectroscopy. As an illustrative example, a hydrogenated amorphous carbon film was analyzed using this method, and showed good agreement with X-ray photoelectron spectroscopy (which is surface sensitive). Furthermore, the results were consistent with analysis from Raman spectroscopy (which is not surface sensitive), indicating the absence of a structurally different near-surface region in this particular thin film material. The present work can assist surface scientists in the analysis of NEXAFS spectra for the accurate characterization of the structure of carbon-based materials.

INTRODUCTION

Both natural and synthetic carbon-based materials exist in a range of forms, including diamond, graphite, graphene and functionalized forms thereof, nanotubes, fullerenes, diamondoids, diamond-like carbon, carbides, polymers, and many other composites[1]. The widespread use of carbon-based materials derives from their excellent properties (*e.g.*, mechanical, electrical, and optical), which are in part due to the ability of carbon to hybridize in multiple bonding states (*i.e.*, sp^3, sp^2, and sp), and to strongly bind to many other elements, such as hydrogen[1]. Due to the strong dependency of the aforementioned properties on the carbon local bonding configuration, the characterization of the structure of carbon-based materials is of paramount importance for engineering materials able to meet the performance and durability requirements of technologically-advanced applications, especially in harsh environments.

Multiple forms of carbon-based materials have found application as very effective protective coatings, including diamond, diamond-like carbon, carbon nitride, and others[2,3]. The impressive properties of these materials, notably their high strength and strain to failure, their ability to withstand certain harsh physical and chemical conditions, and their ability to form smooth, continuous, conformal coatings, have resulted in their use in a range of applications, including those demanding outstanding tribological performance (*i.e.*, low friction, wear, and adhesion)[2]. This includes coatings for high-performance tools[4], hard-disks[5,6], microelectromechanical systems (MEMS)[7], automotive and aerospace components[8,9], and atomic force microscope probes[10].

One of the most well-known classes of carbon-based materials is composed of pure and doped amorphous carbons (a-C). These materials, usually referred to as diamond-like carbon, are deposited by means of chemical or physical vapor deposition methods[11] and consist of a

metastable amorphous arrangement of carbon, in which carbon atoms are present in different hybridization states (mainly sp^3 and sp^2, with a small fraction of sp)[2,11]. Depending on the deposition methodology, conditions, and precursors, hydrogen can also be stably incorporated (up to approximately 50 at.%)[11]. Since the mechanical, chemical, and electronic properties of a-C strongly depend on the hybridization state of carbon atoms, local ordering, and hydrogen content, reliable and accurate structural characterization of a-C films is required to understand, predict, and control materials properties[11]. However, the lack of medium- and long-range order in the atomic network of a-C films, due to the broad range of bond lengths and angles, makes the analysis of their structure challenging.

As a consequence, some of the most powerful weapons in the materials characterization arsenal have been used to characterize these materials[11], including Raman spectroscopy[11-16], X-ray photoelectron spectroscopy (XPS)[16-26], Auger electron spectroscopy (AES, including X-ray induced AES (XAES))[17,18,20,22,23,25,27,28], near edge X-ray absorption fine structure (NEXAFS) spectroscopy[14,21,29-35], electron energy-loss spectroscopy (EELS)[15,36-38], Fourier-transform infrared spectroscopy[39], nuclear magnetic resonance spectroscopy[40], and X-ray reflectivity[15]. Among the surface-sensitive techniques, electron spectroscopies (XPS, AES, XAES, NEXAFS, and EELS) are widely used for the characterization of a-C materials.

XPS is an effective analytical tool for the identification of the elements (except hydrogen and helium[41]) and the quantitative determination of their concentration in the near-surface region of solid surfaces (XPS information depth ranging from 3 nm to 15 nm depending on the element, the material, and the analysis conditions[41]). The characterization of the bonding configuration of carbon is usually carried out by XPS through the acquisition and fitting of the C1s spectrum[16-20,26-28]. However, the validity of the methodology for the quantitative evaluation of the

hybridization state of carbon on the basis of the C1s signal, which relies on fitting it with two distinct features for sp^2- and sp^3-bonded carbon[16,26,27], has been refuted[17,18], since the binding energy values of the C1s transition for graphite (100% sp^2-bonded carbon), diamond (100% sp^3-bonded carbon), and ultrananocrystalline diamond (94±1% sp^3-bonded carbon[21]) are not significantly different[17,18]. Instead, insights into the carbon hybridization state in the near-surface region of a-C materials can be gained by XPS through the analysis of the plasmon band near the C1s signal[18,24], the π-π* shake-up satellites[42,43], or the X-ray induced C KVV Auger spectrum[17,18,22,23,25,28].

Besides XPS, EELS and NEXAFS spectroscopy are effective methods for the determination of the hybridization state of carbon atoms in a-C films[11]. Even though EELS allows the fraction of carbon atoms in sp^2- and sp^3-hybridization state to be quantified through the analysis of the low loss region (from 0 to 40 eV) or the high loss region at the C1s[11,15,36-38], it requires the film to be removed from the substrate or for a cross-section to be produced. Additionally, the acquisition of the C1s is usually carried out with limited energy resolution of approximately 0.5 eV[11,44]. With an energy resolution ≤0.1 eV (depending on the spectrometer) and no sample preparation needed[*], NEXAFS spectroscopy overcomes these two limitations of EELS, which makes it an attractive analytical tool for the study of carbon-based materials.

The power of carbon 1s NEXAFS spectroscopy derives from the resolvable energy difference between the resonant X-ray excitations of a core-level (C1s) electron to unoccupied molecular orbitals (π* or σ*), which allows the identification of the bonding configuration and

---

[*] In the case of photoelectrom emission microscopy (PEEM) measurements coupled with NEXAFS spectroscopy, platinum can be deposited on the sample surface to provide proper grounding and *in situ* normalization for the data acquired on the regions of interests[45,46]. The thickness of the platinum layer on the region of interest needs to be smaller than the information depth at the transition of the element under investigation (to allow photoelectrons emitted from the sample to be detected), whereas on the rest of the specimen it can be larger than the information depth at the transition of the element under investigation.

hybridization state of carbon atoms in the near-surface region of carbon-based materials, such as diamond[45-49], amorphous carbon[14,29,50-52], graphene[53,54], and polymers[55-57]. The dependence of the intensity of the detected spectral features on the orientation of the final state orbital with respect to the electric field vector of the incident photon beam[58] also allows the surface molecular orientation of nanomaterials[59-61] and adsorbates[62] to be investigated.

However, three main sets of challenges exist for the analysis of C1s NEXAFS spectra:

a. energy calibration, intensity normalization, removal of features in as-acquired spectra due to beam instabilities, signal offsets, and beamline transmission function[58,63,64];
b. removal of artifacts in the as-collected data due to the adventitious carbon contamination (subsequently modified by X-ray exposure) of X-ray optics in synchrotron beamlines[64];
c. removal of the contribution of the adventitious contamination layer from the C1s spectra of materials previously exposed to air[21].

Several methods have been reported in the literature for addressing the first two issues. Watts *et al*. reviewed and implemented these approaches with a particular focus on C1s spectra[64]. The third issue derives from the fact that the characterization of the surface chemistry of carbon-based materials by electron yield NEXAFS spectroscopy is usually performed under the assumption of structural and compositional homogeneity within the nanometer-scale depth probed by this technique (for electron yield C1s NEXAFS spectroscopy, the information depth is usually less than 5 nm[58]). The authors of the present work recently demonstrated that this assumption could introduce large errors in the computed carbon hybridization state (between 5% and 20%) when analyzing carbon-based materials previously exposed to air, since the as-acquired C1s NEXAFS spectrum is a convolution of the spectrum of the material under investigation and the spectrum of the adventitious carbon contamination on its surface[21]. The

development and use of a methodology for removing the contribution of thin overlayers from NEXAFS spectra of two-layered systems allowed the authors to compute the contamination-corrected NEXAFS spectra of the substrate, which provided qualitatively distinct interpretations and quantitatively distinct values regarding the sample's composition and bonding compared to the as-acquired data.

In spite of these difficulties, NEXAFS spectroscopy has been extensively applied to quantitatively evaluate the hybridization state of carbon atoms in the near-surface region. However, to the knowledge of the authors, a critical assessment of the methodology for the quantification of the local bonding configuration of carbon on the basis of NEXAFS data is still lacking. Here, we first review this methodology (Section I). Then, we investigate the potential sources of uncertainty and errors (Section II). Finally, in Section III we compare the results of the NEXAFS analysis of an hydrogenated amorphous carbon (a-C:H) film with the outcomes of the characterization of the same material by XPS and Raman spectroscopy.

EXPERIMENTAL

Materials

Hydrogenated amorphous carbon (a-C:H) films (HGST, San Jose, CA, USA) were grown on glass disks coated with 20 nm of NiTa by plasma enhanced chemical vapor deposition from acetylene as gas precursor (NTI source, Intevac Inc., Santa Clara, CA, USA) using an acceleration bias voltage of 180 V. The film thickness was approximately 30 nm (determined by X-ray reflectivity). All samples were cleaned with acetone and ethanol in laboratory air, dried with nitrogen, and stored for several weeks in a nitrogen-purged box before being exposed to

laboratory air for 2 days, and then examined by NEXAFS spectroscopy. The XPS and Raman characterization of these films is reported in Ref. [21] and [13], respectively.

Freshly cleaved highly ordered pyrolytic graphite (HOPG, grade 2, SPI Supplies, West Chester, PA, USA) was used as reference compound for NEXAFS measurements.

Methods

NEXAFS spectroscopic measurements were performed at the NIST/Dow endstation of beamline U7A and at the Oak Ridge National Laboratory endstation of beamline U12A at the National Synchrotron Light Source, Brookhaven National Laboratory (Upton, NY, USA). A detailed description of the experimental procedures for acquiring and processing the NEXAFS data is reported in Ref. [21] and in the Supporting Information.

RESULTS AND DISCUSSION

Section I – Methodology for the quantitative evaluation of the carbon hybridization state by NEXAFS spectroscopy

X-ray absorption spectra are dominated by dipole transitions as in the case of EELS spectra in the limit of small momentum transfer (*i.e.*, for excitation of shells at wavelength >> shell diameter)[58]. Thus, the methodology developed for the determination of the carbon hybridization state from the carbon core loss edge in EELS[36,65] can be applied for the quantitative evaluation of the carbon local bonding configuration on the basis of NEXAFS data. The method, which was qualitatively supported by Car-Parrinello *ab initio* molecular dynamics simulations[66], considers the relative intensity of the C1s$\rightarrow\pi^*$ and C1s$\rightarrow\sigma^*$ absorption features in NEXAFS/EELS spectra of carbon-based materials. Since no theory exists to predict the π^*/σ^* ratio, a reference

material with known sp^2 content is required for quantitative analysis. The equation used to compute the fraction of sp^2-bonded carbon (f_{sp^2}) is:

$$f_{sp^2} = \frac{I^{\pi^*}_{sam} / I_{sam}\left(\Delta E\right)}{I^{\pi^*}_{ref} / I_{ref}\left(\Delta E\right)} \qquad \text{Eq. 1}$$

where $I^{\pi^*}_{sam}$ and $I^{\pi^*}_{ref}$ are, respectively, the areas of the C1s→π* peaks for the sample and the reference (which arise exclusively from sp^2 bonds), whereas $I_{sam}\left(\Delta E\right)$ and $I_{ref}\left(\Delta E\right)$ are the areas under the NEXAFS/EELS spectrum between two integration limits (x_1 and x_2) for the sample and the reference, respectively, as discussed below.

A graphical representation of the methodology is shown in Figure S.1. Since the C1s→π* transition usually appears in NEXAFS spectra of a-C materials as a distinct spectral feature at around 285.0 eV, its area can be determined by fitting it with a Gaussian synthetic peak[21,47]. However, others have computed the area of the C1s→π* feature by integrating the spectrum between 282 and 286 eV[67] or between 282 and 287 eV[30,33,34]. As for the C1s→σ* absorption feature, its area is usually determined by numerically integrating the spectrum between two limits x_1 and x_2, which are chosen to represent the σ* contribution to the experimental data. A survey of the published literature revealed that a wide range of integration limit values (x_1-x_2) has been used for computing the area of the C1s→σ* transition: 289-295 eV[67], 294-301 eV[33,34], 293-302 eV[30], 288.6-325 eV[47], 289-325 eV[46], and 288.6-320 eV[21]. A quantitative assessment of the influence of the integration limits on the computed fraction of sp^2-bonded carbon is presented in Section II.

As a reference, the spectrum of freshly-cleaved HOPG (Figure S.1) sample is commonly employed[21,30,47,52]. One key set of challenges in the use of HOPG as reference material derives

from the strong dependence of the π*/σ* ratio on the orientation of the basal planes with respect to the incoming X-ray beam[58]. Since a theoretical rationale for the experimental settings (*i.e.*, X-ray incidence angle) to be used for the acquisition of a HOPG reference spectrum is missing, HOPG spectra acquired at different X-ray beam incidence angles have been used in the literature. For example, HOPG spectra were acquired at 55° with respect to the sample surface[47], while others were acquired at 45°[21,30]. Section II presents the theoretical derivation of the experimental conditions to be used for the acquisition of a HOPG spectrum to which the π* and σ* states contribute equally (*i.e.*, the conditions under which a molecular orbital oriented normal to the substrate surface contributes the same NEXAFS intensity as the orbital oriented within the substrate plane). In addition, the uncertainty in the fraction of sp^2-bonded carbon due to an uncertainty in the X-ray incidence angle will be discussed.

Since the π*/σ* ratio depends on the angle of the impinging X-ray photons relative to the HOPG basal planes[58], some authors have used other reference materials for quantification, such as fullerene films[32,68], disordered forms of graphite (*e.g.*, Ar^+ sputtered HOPG)[14,33,34], and evaporated carbon[67]. The use of these materials for the quantitative evaluation of the carbon hybridization state from NEXAFS spectra will not be discussed in this work.

Section II – Uncertainties and sources of errors in the quantitative evaluation of the carbon hybridization state by NEXAFS spectroscopy

X-ray incidence angle for the acquisition of the HOPG reference spectrum

HOPG constitutes an ideal system in which the π* and σ* orbitals can be described by a vector ($\vec{O}$, Figure S.2a) and a plane (with normal $\vec{N}$, Figure S.2b), respectively. The π* resonance appears in the NEXAFS spectrum at 285.5 eV, whereas the σ* resonances are detected in the

region between 290 and 305 eV (Figure 1a)[69]. The C1s→π* and C1s→σ* transitions can be respectively thought of as dipole transitions from *s* states to the *p* component of the π* and σ* final states. The corresponding transition matrix elements have a strong angular dependence on the orientation of the final state orbital with respect of the polarization vector of the impinging X-ray photons[58]. Because of that, the intensity of the C1s→π* and C1s→σ* absorption features varies with the X-ray incidence angle (θ)[58], as depicted in Figure 1a. In the following, a theoretical rationale for the X-ray incidence angle to be used for acquiring HOPG spectra to be employed as reference in the quantification of the hybridization state of carbon-based materials is presented.

The angular dependence of the total resonance intensity for the π* orbital (I_{π^*}) and of the resonance intensities associated with the $E^{\parallel}$ ($I_{\pi^*}^{\parallel}$) and $E^{\perp}$ ($I_{\pi^*}^{\perp}$) components can be written as[58]:

$$I_{\pi^*} = PI_{\pi^*}^{\parallel} + (1-P)I_{\pi^*}^{\perp} \qquad \text{Eq. 2a}$$

$$I_{\pi^*}^{\parallel} = \cos^2\theta\cos^2\alpha + \sin^2\theta\sin^2\alpha\cos^2\phi + 2\sin\alpha\cos\alpha\sin\theta\cos\theta\cos\phi \qquad \text{Eq. 2b}$$

$$I_{\pi^*}^{\perp} = \sin^2\alpha\sin^2\phi \qquad \text{Eq. 2c}$$

where P is the polarization factor in the plane of the electron beam orbit ($P = \left|E^{\parallel}\right|^2 / \left(\left|E^{\parallel}\right|^2 + \left|E^{\perp}\right|^2\right)$)[58] (equal to 0.85 for the beamlines used in the present work[62,70]), α is the polar angle, and ϕ is the azimuthal angle (Figure S.2a).

Similarly, the angular dependence of the total resonance intensity for the σ* orbitals (I_{σ^*}) and of the resonance intensities associated with the $E^{\parallel}$ ($I_{\sigma^*}^{\parallel}$) and $E^{\perp}$ ($I_{\sigma^*}^{\perp}$) components can be written as[58]:

$$I_{\sigma^*} = PI_{\sigma^*}^{\parallel} + (1-P)I_{\sigma^*}^{\perp} \qquad \text{Eq. 3a}$$

$$I_{\sigma^*}^{\parallel} = 1 - \cos^2\theta\cos^2\gamma - \sin^2\theta\sin^2\gamma\cos^2\phi - 2\sin\gamma\cos\gamma\sin\theta\cos\theta\cos\phi \quad \text{Eq. 3b}$$

$$I_{\sigma^*}^{\perp} = 1 - \sin^2\gamma\sin^2\phi \quad \text{Eq. 3c}$$

where γ is the angle between the sample normal $\vec{n}$ and the normal $\vec{N}$ of the σ* plane (Figure S.2b).

As shown in the full derivation in the Supporting Information, in the case of HOPG the $\cos^2\phi$ term in Equations 2 and Equations 3 averages to 1/2 because of its three-fold symmetry. Additionally, for HOPG α and γ (Figure S.2) are equal to 0°. Thus, the critical X-ray incidence angle (θ_c), in correspondence of which the π* and σ* transitions equally contribute to the NEXAFS spectrum of HOPG, can be computed:

$$\theta_c = \cos^{-1}\sqrt{\frac{1}{2P}} \quad \text{Eq. 4}$$

In the case of linearly polarized X-rays (P=1), θ_c is equal to 45°, while for elliptically polarized X-rays with polarization factor P equal to 0.85 (as in the case of U7A and U12A), θ_c is equal to 40°. It should be noted that there are claims in the literature that this angle should be the magic angle (*i.e.*, 55° with respect to the sample surface), which was calculated by Stöhr as the X-ray incidence angle at which the measured spectral intensity distribution for the case of organic molecules adsorbed on solid substrates with threefold surface symmetry is independent of the molecular orientation[58]; the analysis above shows this is not the correct angle to use. The above X-ray incidence angles should be used for acquiring HOPG spectra to be employed as reference in the determination of the carbon local bonding configuration from NEXAFS data (using Equation 1).

Uncertainty in X-ray incidence angle of the HOPG reference spectrum

Despite the simplicity of the calculation of the carbon hybridization state on the basis of NEXAFS data (Equation 1), a practical challenge that could make the fraction of sp^2-bonded carbon difficult to accurately quantify is the precise determination of the integrated intensity ratio of the C1s→π* and C1s→σ* absorption features in the HOPG reference spectrum at the critical X-ray incidence angle (θ_c). Since the π*/σ* ratio in HOPG spectra strongly depends on the X-ray incidence angle (θ)[58], uncertainty in the angular position of the HOPG relative to the impinging X-ray photons can lead to errors in the quantitative analysis. Because of that, an uncertainty analysis is needed to determine the uncertainty in the computed fraction of sp^2-bonded carbon. The analysis below, performed following the *Law of Propagation of Uncertainties*[71], assumes that the sample under investigation is isotropic, and either amorphous or polycrystalline (with grain size << X-ray beam diameter), meaning that the π*/σ* ratio for this material does not vary with the X-ray incidence angle.

For the uncertainty analysis, an analytical expression for the dependence of the relative intensity of the C1s→π* and C1s→σ* absorption features in HOPG spectra on the X-ray incidence angle is required. To derive this, the experimentally-determined evolution of the π* and σ* integrated intensities as a function of the X-ray incidence angle was first fit with the following Equations (derived upon substituting Equations S.4 into Equations S.1a and S.2a):

$$I_{\pi^*} = AP\cos^2(\theta+\phi) \qquad \text{Eq. 5a}$$

$$I_{\sigma^*} = C + B\left[1 - P\cos^2(\theta+\phi)\right] \qquad \text{Eq. 5b}$$

where *A* and *B* are two constants that describe the angle-integrated intensity of the two absorption features, C is a constant accounting for the fact that the area of the C1s→σ* transition is calculated by integrating the spectrum between two limits (x_1 and x_2) without

subtracting any absorption edge, and ϕ is a phase constant accounting for any misalignment in the angular position of HOPG. The experimental data in Figure 1b could be well fit by Equations 5 using A, B, C, and ϕ as fitting parameters.

Based on Equation 5a and 5b, an expression describing the dependence of the π*/σ* ratio on the X-ray incidence angle can be readily derived:

$$\frac{I_{\pi^*}}{I_{\sigma^*}} = \frac{AP\cos^2(\theta+\phi)}{C + B\left[1 - P\cos^2(\theta+\phi)\right]} \quad \text{Eq. 6}$$

Since A, B, and C were determined from individually fitting the evolution of the integrated intensities of the C1s→π* and C1s→σ* transitions with the X-ray incidence angle (Figure 1b), the fit of the π*/σ* ratio can be performed using only one fitting parameter, *i.e.*, the phase constant ϕ. As displayed in Figure 1c, Equation 6 fits the experimental data well.

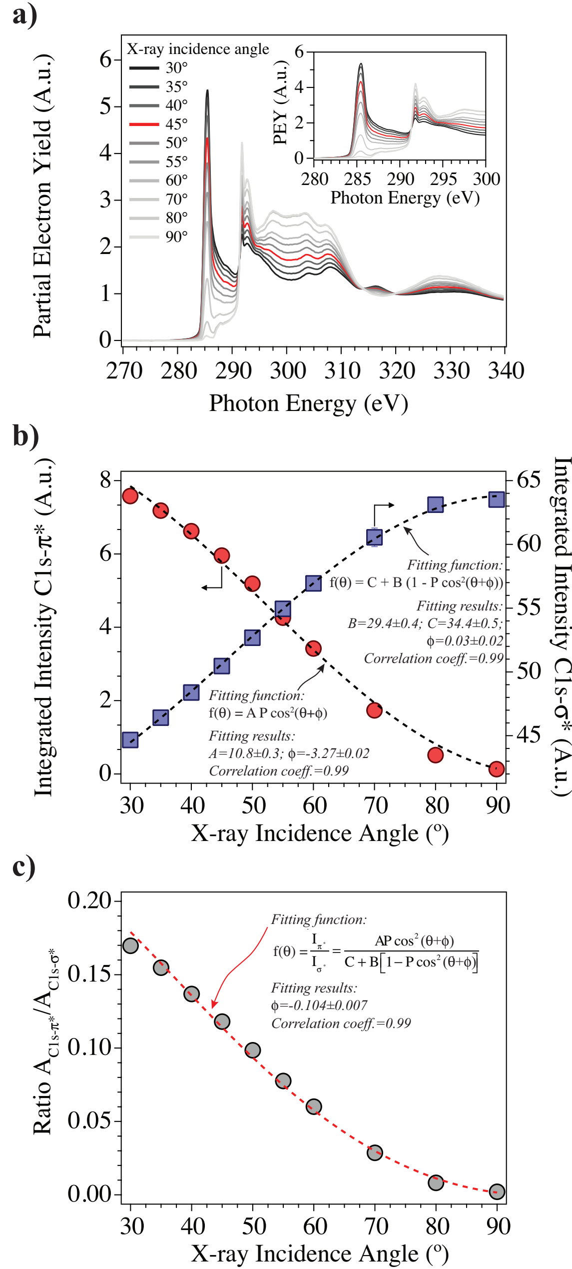

Figure 1. (a) C1s NEXAFS spectra of HOPG acquired at different X-ray incidence angles. Inset: zoomed view of the absorption edge region of the C1s spectra. Spectra displayed without any offset to allow for comparisons; (b) integrated intensity of the C1s→π* (computed by fitting this signal with a Gaussian synthetic peak) and C1s→σ* (computed by numerically integrating the spectrum between 288.6 and 320 eV) absorption features as a function of the X-ray incidence

angle. The experimental data are well fit using Equations 5a and 5b (dashed lines); (c) ratio of the integrated intensity of the C1s$\rightarrow\pi^*$ (computed by fitting this signal with a Gaussian synthetic peak) and C1s$\rightarrow\sigma^*$ (computed by numerically integrating the spectrum between 288.6 and 320 eV) absorption features as a function of the X-ray incidence angle. The experimental data are well fit using Equation 6 (red dashed line).

The analytical expression obtained from the fit to the experimental data was used for calculating the uncertainty in the fraction of sp^2-bonded carbon due to uncertainties in the X-ray incidence angle (Figure 2). The uncertainty increases with both the fraction of sp^2-bonded carbon (Figure 2a) and the uncertainty in the angle of X-ray incidence (Figure 2b). In the case of the beamlines used in this work, the uncertainty in the X-ray incidence angle was 1°, which translates into an uncertainty in the computed fraction of sp^2-bonded carbon linearly increasing with the fraction of sp^2-bonded carbon up to 3.6% for 100% sp^2-bonded carbon, which is modest. However, a larger uncertainty in X-ray incidence angle of 5° produces a much more significant error of 8.9% for 50% sp^2-bonded carbon, and 17.9% for 100% sp^2-bonded carbon.

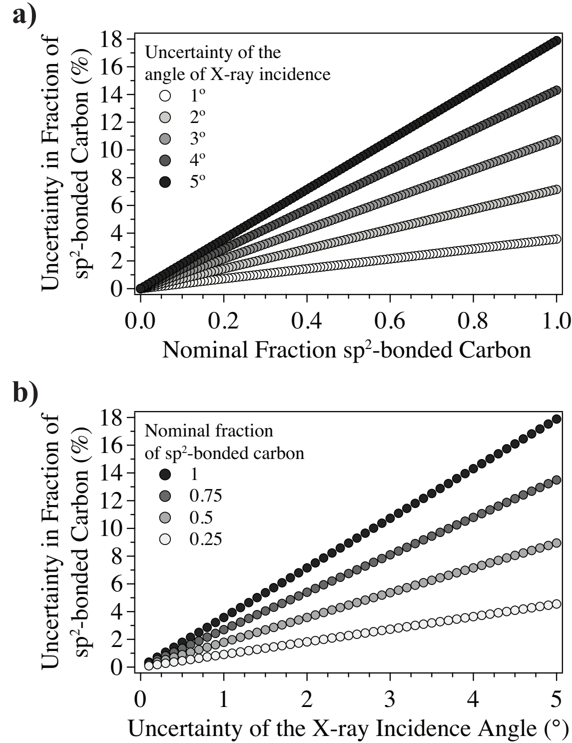

Figure 2. Uncertainty in the computed fraction of sp^2-bonded carbon due to uncertainties in the X-ray incidence angle for the HOPG reference spectrum as a function of: (a) the nominal fraction of sp^2-bonded carbon; and (b) the uncertainty in the X-ray incidence angle.

<u>Integration limits for calculating the integrated intensity of the C1s→σ* transition</u>

The intensity of the C1s→σ* absorption feature in NEXAFS spectra is normally computed by numerically integrating the spectrum between two limits x_1 and x_2, which are chosen to represent the σ* contribution to the experimental data. A literature survey revealed that a wide range of integration limits has been used (as mentioned previously in Section I). Thus, the effect of the integration limits on the computed fraction of sp^2-bonded carbon was investigated.

Figure 3 displays the evolution of the computed fraction of sp^2-bonded carbon for an a-C:H film as a function of the integration limits used to calculate the area of the C1s→σ* transition.

For highlighting the influence of the integration limits on the results of the quantification, the error in the calculated fraction of sp^2-bonded carbon relative to the fraction obtained using the integration limits employed in Ref. [21] (x_1=288.6 eV; x_2=320 eV) is also shown in Figure 3.

Upon varying the low-photon-energy integration limit (x_1) between 286.6 and 295 eV while keeping the high-photon-energy integration limit at 320 eV, no significant variations in the computed fraction of sp^2-bonded carbon were observed (Figure 3a). On the contrary, significant variations, as large as 10%, in the fraction of sp^2-hybridized carbon were found upon decreasing the high-photon-energy integration limit (x_2) below 310 eV (while keeping the low-photon-energy integration limit at 288.6 eV) (Figure 3b). Thus, for the quantification of the carbon hybridization state using carbon 1s NEXAFS spectroscopy, the low-photon-energy integration limit (x_1) can be chosen arbitrarily between 286.6 eV and 295 eV, whereas the high-photon-energy integration limit (x_2) should be taken at photon energies above 310 eV.

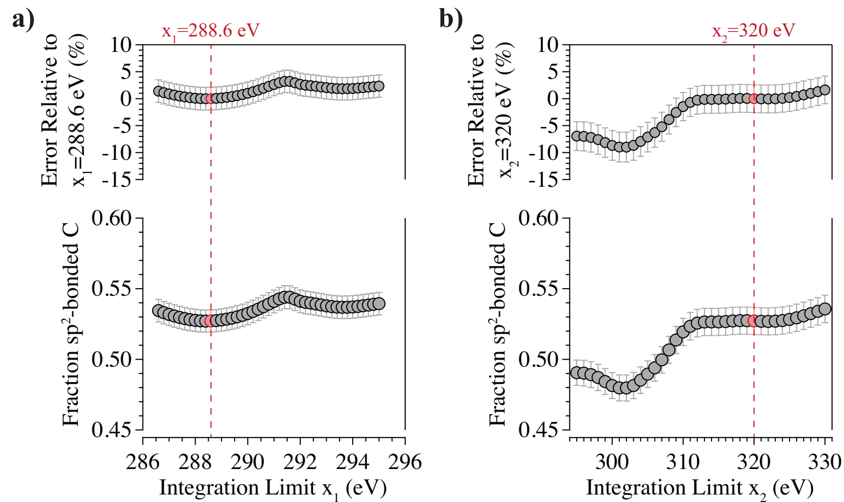

Figure 3. (a) Influence of the lower-photon-energy integration limit x_1 used to calculate the area of the C1s→σ* transition on the computed fraction of sp^2-bonded carbon for a hydrogenated amorphous carbon film (the high-photon-energy limit x_2 was kept fixed at 320 eV). Error bars

represent the standard deviation calculated from multiple independent measurements; (b) influence of the high-photon-energy integration limit x_2 used to calculate the area of the C1s→σ* transition on the computed fraction of sp^2-bonded carbon for a hydrogenated amorphous carbon film (the low-photon-energy limit x_1 was kept fixed at 288.6 eV). Error bars represent the standard deviation calculated from multiple independent measurements. For highlighting the influence of the integration limits on the results of the quantification, the error in the calculated fraction of sp^2-bonded carbon relative to the fraction obtained using the integration limits employed in Ref. [21] (x_1=288.6 eV; x_2=320 eV) is shown in the upper part of the graphs.

Section III – Comparison between NEXAFS, XPS, and Raman spectroscopic results

Table 1 reports the results of the quantitative evaluation of the carbon hybridization state for an a-C:H film performed on the basis of NEXAFS, XPS, and Raman spectroscopy. The fraction of sp^2-bonded carbon computed from NEXAFS spectroscopic data in which the HOPG reference spectrum is acquired at θ_c=40°, agrees, within uncertainty, with the outcomes of the XPS and Raman characterization. On the contrary, the use of the HOPG spectrum acquired at θ_c=45° as reference (*i.e.*, when the X-ray are assumed to be linearly polarized (*P*=1)) results in a numerical value for the fraction of sp^2-hybridized carbon that is still not significantly different than the ones obtained by XPS, but is slightly higher than the outcomes of Raman measurements. Since there are claims in the literature that the HOPG reference spectrum should be acquired at magic angle (*i.e.*, 55° with respect to the sample surface), for completeness we calculated the fraction of sp^2-bonded carbon using the HOPG spectrum collected at θ_c=55° as reference. The outcome of this analysis is substantially different from the results of XPS and Raman measurements and from the NEXAFS analysis performed at the correct incidence angle of 40°. This highlights the

importance of using the correct angle of incidence of the X-ray beam when acquiring HOPG reference spectra.

Table 1. Fraction of sp^2-bonded carbon determined from NEXAFS, XPS, and Raman spectroscopy.

NEXAFS spectroscopy			***XPS*****		***Raman spectroscopy[13]***
HOPG reference spectrum acquired at θ_c=40°	*HOPG reference spectrum acquired at θ_c=45° **	*HOPG reference spectrum acquired at θ_c=55°*	*Analysis of the plasmon band near C1s core level signal[18]*	*Analysis of the X-ray induced C KVV Auger spectrum[17-19]*	
0.44±0.03	0.50±0.03	0.77±0.03	0.48±0.04	0.48±0.02	0.45±0.01

* this value agrees, within uncertainty, with the one reported in Ref. [21], which was obtained from samples from a different deposition run.

** these values agree, within uncertainty, with the ones reported in Ref. [18], which were obtained from samples from a different deposition run.

Finally, it is important to emphasize that the information gained by analytical methods with different surface sensitivity can potentially differ due to the presence of structurally different near-surface regions. Depending on the synthesis and growth conditions, carbon-based materials can exhibit gradients in their structure or well-defined layers with completely different local bonding configurations of carbon[72,73]. The comparison between the NEXAFS results presented herein (information depth for the analyses performed at U7A: 3.8 nm[21]) with Raman (optical mean free path at 514.5 nm wavelength for a-C:H films: >200 nm[74]) and XPS (information depth for the plasmon band: 9.5 nm; information depth for C KVV signal: 3.3 nm[18]) measurements

provides experimental evidence that a structurally different near-surface region is not present for the film under investigation. Such a conclusion could not be reached without the accurate quantitative evaluation of the carbon hybridization state by NEXAFS spectroscopy.

CONCLUSIONS

The methodology for quantitatively evaluating the carbon local bonding configuration on the basis of NEXAFS spectroscopic measurements, which is based on the analysis of the sample of interest and of a reference spectrum (usually HOPG), was reviewed. The critical assessment of this method allowed the identification of the experimental conditions to be used for the acquisition of suitable HOPG reference spectra as well as the potential sources of uncertainty and errors in the computed fraction of sp^2-bonded carbon. In particular, we show that it is important to use the correct angle of incidence of the X-ray beam when acquiring HOPG reference spectra and to minimize the uncertainty in this angle. Additionally, the integration limits used to calculate the area of the C1s $\rightarrow \sigma^*$ transition should be carefully selected; otherwise, variations as large as 10% in the computed fraction of sp^2-hybridized carbon can result. The comparison of the NEXAFS characterization of a hydrogenated amorphous carbon film, corrected for carbon surface contamination, with the outcomes of XPS and Raman measurements revealed good agreement between the analytical results, which validates the method and further indicates the absence of a structurally different near-surface region in this thin-film material. The present work can help surface scientists employ NEXAFS spectroscopy for the accurate characterization of the structure of carbon-based materials.

ASSOCIATED CONTENT

Supporting Information. A detailed description of the experimental procedures for acquiring and processing NEXAFS data is reported. A graphical representation of the methodology for the quantitative evaluation of the carbon hybridization state by NEXAFS spectroscopy is shown. A full derivation of the experimental conditions to be used for the acquisition of HOPG reference spectra is reported. This material is available free of charge via the Internet at http://pubs.acs.org.

AUTHOR INFORMATION

Corresponding Author

*Email: f.mangolini@leeds.ac.uk

Notes

The authors declare no competing financial interests.

ACKNOWLEDGMENTS

This material is based upon work supported by the Advanced Storage Technology Consortium ASTC (grant 2011-012) and the National Science Foundation under Grant No. DMR-1107642. F.M. acknowledges support from the Marie Curie International Outgoing Fellowship for Career Development under contract no. PIOF-GA-2012-328776. The authors would like to thanks Dr. C. Jaye, Dr. D.A. Fischer, Dr. P. Albrecht, and Dr. D.R. Mullins for their kind assistance with the NEXAFS measurements at the National Synchrotron Light Source. Use of the National Synchrotron Light Source, Brookhaven National Laboratory, was supported by the US Department of Energy, Office of Science, Office of Basic Energy Sciences, under Contract No.

DE-AC02-98CH10886. We are grateful to Dr. F. Rose (previously at HGST, a Western Digital Company) for the X-ray reflectivity and Raman measurements. We acknowledge Prof. J. Stöhr from Stanford University and Dr. J. Fontaine from École Centrale de Lyon for fruitful discussions.

REFERENCES

(1) Krüger, A. *Carbon materials and nanotechnology*; John Wiley & Sons: New York, 2010, p 490.

(2) Donnet, C.; Erdemir, A. *Tribology of Diamond-Like Carbon Films*; Springer: New York, 2008, p 664.

(3) Erdemir, A.; Donnet, C. In *Modern Tribology Handbook*, Bhushan, B., Ed.; CRC Press: Boca Raton, 2001.

(4) Heaney, P. J.; Sumant, A. V.; Torres, C. D.; Carpick, R. W.; Pfefferkorn, F. E. *Diamond Relat. Mater.* **2008**, *17*, 223-233.

(5) Ferrari, A. C. *Surf. Coat. Technol.* **2004**, *180-181*, 190-206.

(6) Marchon, B. *J. Appl. Phys.* **1996**, *79*, 4508-4508.

(7) Auciello, O.; Birrell, J.; Carlisle, J. A.; Gerbi, J. E.; Xiao, X.; Peng, B.; Espinosa, H. D. *J. Phys.: Condens. Matter* **2004**, *16*, R539.

(8) Tung, S. C.; McMillan, M. L. *Trib. Int.* **2004**, *37*, 517-536.

(9) Fontaine, J. *Proc. Inst. Mech. Eng. J J. Eng. Tribol.* **2008**, *222*, 1015-1029.

(10) Liu, J.; Grierson, D. S.; Moldovan, N.; Notbohm, J.; Li, S.; Jaroenapibal, P.; O'Connor, S. D.; Sumant, A. V.; Neelakantan, N.; Carlisle, J. A.; Turner, K. T.; Carpick, R. W. *Small* **2010**, *6*, 1140-1149.

(11) Robertson, J. *Mat. Sci. Eng. R Rep.* **2002**, *37*, 129-281.

(12) Ferrari, A. C.; Robertson, J. *Phil. Trans. R. Soc. A* **2004**, *362*, 2477-2512.

(13) Rose, F.; Wang, N.; Smith, R.; Xiao, Q.-F.; Inaba, H.; Matsumura, T.; Saito, Y.; Matsumoto, H.; Dai, Q.; Marchon, B.; Mangolini, F.; Carpick, R. W. *J. Appl. Phys.* **2014**, *116*, 123516.

(14) Lenardi, C.; Piseri, P.; Briois, V.; Bottani, C. E.; Bassi, A. L.; Milani, P. *J. Appl. Phys.* **1999**, *85*, 7159-7167.

(15) Ferrari, A. C.; Kleinsorge, B.; Adamopoulos, G.; Robertson, J.; Milne, W. I.; Stolojan, V.; Brown, L. M.; LiBassi, A.; Tanner, B. K. *J. Non-Cryst. Solids* **2000**, *266-269, Part 2*, 765-768.

(16) Filik, J.; May, P. W.; Pearce, S. R. J.; Wild, R. K.; Hallam, K. R. *Diamond Relat. Mater.* **2003**, *12*, 974-978.

(17) Kaciulis, S. *Surf. Interface Anal.* **2012**, *44*, 1155–1161.

(18) Mangolini, F.; Rose, F.; Hilbert, J.; Carpick, R. W. *Appl. Phys. Lett.* **2013**, *103*, 161605.

(19) Mezzi, A.; Kaciulis, S. *Surf. Interface Anal.* **2010**, *42*, 1082-1084.

(20) Lascovich, J. C.; Rosato, V. *Appl. Surf. Sci.* **1999**, *152*, 10-18.

(21) Mangolini, F.; McClimon, J. B.; Rose, F.; Carpick, R. W. *Anal. Chem.* **2014**, *86*, 12258-12265.

(22) Kaciulis, S.; Mezzi, A.; Calvani, P.; Trucchi, D. M. *Surf. Interface Anal.* **2014**, *46*, 966-969.

(23) Lesiak, B.; Zemek, J.; Jiricek, P.; Stobinski, L.; Jóźwik, A. *Phys. Status Solidi B* **2010**, *247*, 2838-2842.

(24) Speranza, G.; Laidani, N. *Diamond Relat. Mater.* **2004**, *13*, 445-450.

(25) Zemek, J.; Zalman, J.; Luches, A. *Appl. Surf. Sci.* **1998**, *133*, 27-32.

(26) Diaz, J.; Paolicelli, G.; Ferrer, S.; Comin, F. *Phys. Rev. B* **1996**, *54*, 8064-8069.

(27) Mizokawa, Y.; Miyasato, T.; Nakamura, S.; Geib, K. M.; Wilmsen, C. W. *Surf. Sci.* **1987**, *182*, 431-438.

(28) Mizokawa, Y.; Miyasato, T.; Nakamura, S.; Geib, K. M.; Wilmsen, C. W. *J. Vac. Sci. Technol. A* **1987**, *5*, 2809-2813.

(29) Grierson, D. S.; Sumant, A. V.; Konicek, A. R.; Friedmann, T. A.; Sullivan, J. P.; Carpick, R. W. *J. Appl. Phys.* **2010**, *107*, 033523-033525.

(30) Osswald, S.; Yushin, G.; Mochalin, V.; Kucheyev, S. O.; Gogotsi, Y. *J. Am. Chem. Soc.* **2006**, *128*, 11635-11642.

(31) Coffman, F. L.; Cao, R.; Pianetta, P. A.; Kapoor, S.; Kelly, M.; Terminello, L. J. *Appl. Phys. Lett.* **1996**, *69*, 568-570.

(32) Díaz, J.; Anders, S.; Zhou, X.; Moler, E. J.; Kellar, S. A.; Hussain, Z. *Phys. Rev. B* **2001**, *64*, 125204.

(33) Gago, R.; Jiménez, I.; Albella, J. M. *Surf. Sci.* **2001**, *482–485, Part 1*, 530-536.

(34) Gago, R.; Jiménez, I.; Albella, J. M.; Climent-Font, A.; Cáceres, D.; Vergara, I.; Banks, J. C.; Doyle, B. L.; Terminello, L. J. *J. Appl. Phys.* **2000**, *87*, 8174-8180.

(35) Lenardi, C.; Marino, M.; Barborini, E.; Piseri, P.; Milani, P. *Eur. Phys. J. B* **2005**, *46*, 441-447.

(36) Berger, S. D.; McKenzie, D. R.; Martin, P. J. *Philos. Mag. Lett.* **1988**, *57*, 285-290.

(37) Kulik, J.; Lempert, G. D.; Grossman, E.; Marton, D.; Rabalais, J. W.; Lifshitz, Y. *Phys. Rev. B* **1995**, *52*, 15812-15822.

(38) Wang, Y.; Chen, H.; Hoffman, R. W.; Angus, J. C. *J. Mater. Res.* **1990**, *5*, 2378-2386.

(39) Paterson, M. J. *Diamond Relat. Mater.* **1998**, *7*, 908-915.

(40) Donnet, C.; Fontaine, J.; Lefebvre, F.; Grill, A.; Patel, V.; Jahnes, C. *J. Appl. Phys.* **1999**, *85*, 3264-3270.

(41) Briggs, D.; Grant, J. T. *Surface Analysis by Auger and X-Ray Photoelectron Spectroscopy*; IM Publications: Chichester (UK), 2003, p 899.

(42) Kovach, G.; Karacs, A.; Radnoczi, G.; Csorbai, H.; Guczi, L.; Veres, M.; Koos, M.; Papadimitriou, L.; Sólyom, A.; Pető, G. *Appl. Surf. Sci.* **2008**, *254*, 2790-2796.

(43) Leiro, J. A.; Heinonen, M. H.; Laiho, T.; Batirev, I. G. *J. Electron Spectrosc. Relat. Phenom.* **2003**, *128*, 205-213.

(44) Egerton, R. F. In *Electron Energy-Loss Spectroscopy in the Electron Microscope*; Springer US, 2011, pp 1-28.

(45) Konicek, A.; Jaye, C.; Hamilton, M.; Sawyer, W.; Fischer, D.; Carpick, R. *Trib. Lett.* **2011**, *44*, 99-106.

(46) Konicek, A. R.; Grierson, D. S.; Gilbert, P. U. P. A.; Sawyer, W. G.; Sumant, A. V.; Carpick, R. W. *Phys. Rev. Lett.* **2008**, *100*, 235502.

(47) Sumant, A. V.; Gilbert, P. U. P. A.; Grierson, D. S.; Konicek, A. R.; Abrecht, M.; Butler, J. E.; Feygelson, T.; Rotter, S. S.; Carpick, R. W. *Diamond Relat. Mater.* **2007**, *16*, 718-724.

(48) Sumant, A. V.; Grierson, D. S.; Gerbi, J. E.; Birrell, J.; Lanke, U. D.; Auciello, O.; Carlisle, J. A.; Carpick, R. W. *Adv. Mater.* **2005**, *17*, 1039-1045.

(49) Li, Y. S.; Tang, Y.; Yang, Q.; Maley, J.; Sammynaiken, R.; Regier, T.; Xiao, C.; Hirose, A. *ACS Appl. Mater. Interfaces* **2010**, *2*, 335-338.

(50) Diaz, J.; Anders, S.; Zhou, X.; Moler, E. J.; Kellar, S. A.; Hussain, Z. *J. Electron Spectrosc. Relat. Phenom.* **1999**, *101-103*, 545-550.

(51) Gago, R.; Jimenez, I.; Albella, J. M.; Climent-Font, A.; Caceres, D.; Vergara, I.; Banks, J. C.; Doyle, B. L.; Terminello, L. J. *J. Appl. Phys.* **2000**, *87*, 8174-8180.

(52) Saikubo, A.; Yamada, N.; Kanda, K.; Matsui, S.; Suzuki, T.; Niihara, K.; Saitoh, H. *Diamond Relat. Mater.* **2008**, *17*, 1743-1745.

(53) Schultz, B. J.; Patridge, C. J.; Lee, V.; Jaye, C.; Lysaght, P. S.; Smith, C.; Barnett, J.; Fischer, D. A.; Prendergast, D.; Banerjee, S. *Nat. Commun.* **2011**, *2*, 372.

(54) Pacilé, D.; Papagno, M.; Rodríguez, A. F.; Grioni, M.; Papagno, L.; Girit, Ç. Ö.; Meyer, J. C.; Begtrup, G. E.; Zettl, A. *Phys. Rev. Lett.* **2008**, *101*, 066806.

(55) Kikuma, J.; Tonner, B. P. *J. Electron Spectrosc. Relat. Phenom.* **1996**, *82*, 53-60.

(56) Watts, B.; Swaraj, S.; Nordlund, D.; Luning, J.; Ade, H. *J. Chem. Phys.* **2011**, *134*, 024702.

(57) Park, D.; Finlay, J. A.; Ward, R. J.; Weinman, C. J.; Krishnan, S.; Paik, M.; Sohn, K. E.; Callow, M. E.; Callow, J. A.; Handlin, D. L.; Willis, C. L.; Fischer, D. A.; Angert, E. R.; Kramer, E. J.; Ober, C. K. *ACS Appl. Mater. Interfaces* **2010**, *2*, 703-711.

(58) Stöhr, J. *NEXAFS Spectroscopy*; Springer-Verlag, 1992, p 403.

(59) Hemraj-Benny, T.; Banerjee, S.; Sambasivan, S.; Balasubramanian, M.; Fischer, D. A.; Eres, G.; Puretzky, A. A.; Geohegan, D. B.; Lowndes, D. H.; Han, W.; Misewich, J. A.; Wong, S. S. *Small* **2006**, *2*, 26-35.

(60) Maruyama, T.; Sakakibara, S.; Naritsuka, S.; Amemiya, K. *Diamond Relat. Mater.* **2011**, *20*, 1325-1328.

(61) Winter, A. D.; Larios, E.; Alamgir, F. M.; Jaye, C.; Fischer, D.; Campo, E. M. *Langmuir* **2013**, *29*, 15822-15830.

(62) Genzer, J.; Kramer, E. J.; Fischer, D. A. *J. Appl. Phys.* **2002**, *92*, 7070-7079.

(63) Schöll, A.; Zou, Y.; Schmidt, T.; Fink, R.; Umbach, E. *J. Electron Spectrosc. Relat. Phenom.* **2003**, *129*, 1-8.

(64) Watts, B.; Thomsen, L.; Dastoor, P. C. *J. Electron Spectrosc. Relat. Phenom.* **2006**, *151*, 105-120.

(65) Fallon, P. J.; Veerasamy, V. S.; Davis, C. A.; Robertson, J.; Amaratunga, G. A. J.; Milne, W. I.; Koskinen, J. *Phys. Rev. B* **1993**, *48*, 4777-4782.

(66) McCulloch, D. G.; McKenzie, D. R.; Goringe, C. M. *Phys. Rev. B* **2000**, *61*, 2349-2355.

(67) Gago, R.; Vinnichenko, M.; Jäger, H. U.; Belov, A. Y.; Jiménez, I.; Huang, N.; Sun, H.; Maitz, M. F. *Phys. Rev. B* **2005**, *72*, 014120.

(68) Papworth, A. J.; Kiely, C. J.; Burden, A. P.; Silva, S. R. P.; Amaratunga, G. A. J. *Phys. Rev. B* **2000**, *62*, 12628-12631.

(69) Banerjee, S.; Hemraj-Benny, T.; Sambasivan, S.; Fischer, D. A.; Misewich, J. A.; Wong, S. S. *J. Phys. Chem. B* **2005**, *109*, 8489-8495.

(70) Sohn, K. E.; Dimitriou, M. D.; Genzer, J.; Fischer, D. A.; Hawker, C. J.; Kramer, E. J. *Langmuir* **2009**, *25*, 6341-6348.

(71) Taylor, J. R. *An Introduction to Error Analysis: The Study of Uncertainties in Physical Measurements*; University Science Book: Sausalito, 1997, p 305.

(72) Wang, N.; Komvopoulos, K. *J. Mater. Res.* **2013**, *28*, 2124-2131.

(73) De Barros Bouchet, M. I.; Matta, C.; Vacher, B.; Le-Mogne, T.; Martin, J. M.; von Lautz, J.; Ma, T.; Pastewka, L.; Otschik, J.; Gumbsch, P.; Moseler, M. *Carbon* **2015**, *87*, 317-329.

(74) Scharf, T. W.; Singer, I. L. *Trib. Lett.* **2003**, *14*, 137-145.

TOC GRAPHICS

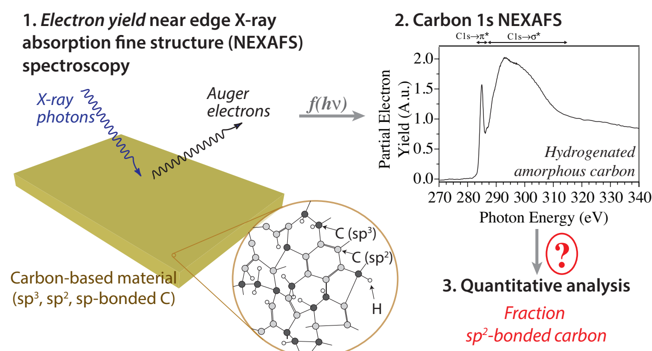

KEYWORDS: Near-edge X-ray absorption fine structure spectroscopy; NEXAFS; carbon-based materials.